Chinese Chemical Letters 33 (2022) 5213–5217

Contents lists available at ScienceDirect

Chinese Chemical Letters

journal homepage: www.elsevier.com/locate/cclet

An insight into aggregation kinetics of polystyrene nanoplastics interaction with metal cations

Yucheng Zhang[a], Xiaotong Su[a], Nora F.Y. Tam[b,c], Xiaolan Lao[a], Meiling Zhong[a], Qihang Wu[a,*], Huifang Lei[a], Zihui Chen[a], Zhang Li[d], Jie Fu[d,*]

[a] Key Laboratory for Water Quality and Conservation of the Pearl Stream Delta, Ministry of Education, School of Environmental Science and Engineering, Guangzhou University, Guangzhou 510006, China
[b] State Key Laboratory of Marine Pollution and Department of Chemistry, City University of Hong Kong, Hong Kong, China
[c] School of Science and Technology, Open University of Hong Kong, Hong Kong, China
[d] School of Environmental Science and Engineering, Huazhong University of Science and Technology, Wuhan 430074, China

ARTICLE INFO

Article history:
Received 15 November 2021
Revised 19 December 2021
Accepted 21 January 2022
Available online 24 January 2022

Keywords:
Polystyrene nanoplastics
Lead cation
Aggregation kinetics
Critical coagulation concentration
Size effect

ABSTRACT

Once inevitably released into the aquatic environment, polystyrene nanoplastics (PS-NPs) will present complicated environmental behaviors, of which the aggregation is a key process determining their environmental fate and impact. In this study, the aggregation kinetics of different sizes (30 nm and 100 nm) of PS-NPs with metal cations (Na^+, K^+, Ca^{2+}, Mg^{2+} and Pb^{2+}) at different solution pH (3, 6 and 8) were investigated. The results showed that the aggregation of PS-NPs increased with cation concentration. Taking Pb^{2+} as an example, the adsorption behavior of cations onto PS-NPs was determined by transmission electron microscopy (TEM) and energy dispersive X-ray (EDX) spectroscopy, which demonstrated Pb^{2+} could be adhered onto the surface of PS-NPs with the effect of charge neutralization. The critical coagulation concentrations (CCC) of smaller PS-NPs were higher than that of larger PS-NPs for monovalent cations, whereas a different pattern is observed for divalent cations. It was suggested that there were other factors that DLVO theory does not consider affect the stability of NPs with different particle sizes. In addition, it should be noted that PS-NPs had the capacity of adsorbing large amounts of heavy metal cations and carried them transport to a long distance, and the corresponding ecological risks need to further elucidate.

Plastics, known as revolutionary materials, have been widely used in various fields since their birth in 1905 [1]. The global consumption of plastics is growing at an annual rate of 4%, increasing from 1.3 million tons in 1950 to 322 million tons in 2015, and then reaching 369 million tons in 2018 [2]. Due to the failure of effective collection, disposal and control of plastic wastes, some plastic fragments or particles are discharged into the natural environment, affecting the normal operation of the ecosystem. Plastic particles with a size less than 100 nm, called nanoplastics, are supposed to be a new type of contaminant, which have ignited the research passion of scholars around the world over the last decade [3]. On one hand, nanoplastics from cosmetics, personal hygiene products, and industrial products such as 3D printing and nanocapsules are constantly released into the environment during their use and production [4]. On the other hand, polymer-based materials are easy to degrade into plastic fragments under the action of high salinity, light, heat and microorganisms [5].

The biological effects of nanoparticles are closely related to particle size. Moore [6] found that the bioavailability of microplastics was largely affected by their particle size. There is a growing body of literature that recognizes the toxic effects of nanoplastics on hydrobiont, which were mainly evaluated through energy consumption, oxidative damage, enzyme activity, reproduction and growth rate [7–9]. Some researchers believe that the aggregation behavior of nanoplastics in water environment is one of the main factors affecting their environmental migration and biological toxicity, and thus focus on the colloidal stability and aggregation dynamics of nanoplastics [10,11]. Surface chemical properties of nanoplastics play an important role in colloid aggregation, and ultimately affect their behavior and fate in water environment [12]. Yu *et al.* [13] have investigated the aggregation of a series of surface-modified polystyrene nanoplastics, and found that the negatively charged and positively charged nanoplastics exhibited different aggregation behaviors. In addition, it has previously been observed

* Corresponding authors.
E-mail addresses: wuqihang@gzhu.edu.cn (Q. Wu), jiefu@hust.edu.cn (J. Fu).

https://doi.org/10.1016/j.cclet.2022.01.056
1001-8417/

that solution properties such as pH, ionic strength, and valence of ions influence the colloidal stability and aggregation behavior of nanoparticles [14]. Metal cations have been demonstrated to significantly affect the stability of nanoplastics when they are adhered on nanoplatics [15–17]. Conversely, nanoplastics can adsorb large amounts of metal cations in heavy metals polluted water, and carry them to migrate, posing a greater potential risk [17].

In this study, two commercial polystyrene nanoplastics (PS-NPs) with different sizes, 30 nm representing small size (PS-S) and 100 nm representing large size (PS-L), were used as model nanoplastics to systematically explore their aggregation kinetics in water with monovalent (Na^+ and K^+) and divalent (Ca^{2+}, Mg^{2+} and Pb^{2+}) metal cations. Polystyrene is one of the most widely used plastic materials [18], and Pb^{2+} is also a common ion in heavy metal polluted water [19]. The attachment efficiencies and critical coagulation concentrations of PS-NPs under different conditions were calculated. The research purpose is to reveal the important roles of particle size and metal cations in the aggregation process of nanoplastics. The provided information could improve the understanding of the environmental behavior and ecological risks of nanoplastics.

The PS-S-NPs suspension (1.0% w/v, 15 mL, 30 nm) was obtained from Thermo Fisher Scientific (Shanghai, China), and PS-L-NPs suspension (2.5% w/v, 10 mL, 100 nm) was purchased from Tianjin BaseLine ChromTech Research Center (Tianjin, China). The NaCl, KCl, $MgCl_2$, $CaCl_2$ and $Pb(NO_3)_2$ of analytical grade were used as the experimental electrolytes. The solution pH was adjusted using 0.1 mol/L HCl and 0.1 mol/L NaOH (Titrisol, Merck, Austria). All the nanoplastics suspensions were diluted to about 10 mg/L with ultrapure water (18.2 MΩ, Milli-Q, Millipore). After adding different concentrations of electrolytes and adjusting to the desired pH, the experimental nanoplastics suspensions were prepared. The hydrodynamic diameter and zeta potential of each sample were measured by dynamic light scattering (DLS) with a 90° scattering angle (ZetaPALS/BI-90 Plus, Brookhaven Instruments Corp., New York, USA). The suspension temperature was maintained at 25 °C. The characteristic of PS-NPs before and after experiments were visualized using a TecnaiG2F20 S-Twin transmission electron microscope (TEM, FEI, USA). The distribution of elemental composition was analyzed by an energy-dispersive X-ray spectroscopy (EDX) system (X-MaxN 80T, Oxford Instruments NanoAnalysis, USA). Fourier transform-infrared (FT-IR) spectra were performed to identify the structural and functional groups of PS-NPs.

The initial aggregation rate constant of PS-NPs (k) is proportional to the change of hydrodynamic diameter (D_h) from the time-resolved DLS measurements with respect to time (t), but inversely proportional to the primary particle concentration of PS-NPs (C) (Eq. 1) [20]:

$$k \propto \frac{\left(\frac{dD_h(t)}{dt}\right)_{t\to 0}}{C} \tag{1}$$

In aggregation experiments, the C was maintained at 10 mg/L. $(\frac{dD_h(t)}{dt})_{t\to 0}$ can be acquired by performing the linear least-squares regression for the initial increase in $D_h(t)$ with t. For most experiments, the regression analysis was performed over a time from $D_h(0)$ to $1.3D_h(0)$, where $D_h(0)$ represented the initial D_h. Under some unfavorable conditions that $D_h(t)$ fail to reach $1.3D_h$ (0), the aggregation of PS-NPs was negligible and $(\frac{dD_h(t)}{dt})_{t\to 0}$ was determined with the achieved maximum $D_h(t)$. For some extremely fast aggregation that $D_h(t)$ may go beyond $1.3D_h(0)$ when experiment has just begun, only the points that showed a linear relationship were chosen to calculate the aggregation rate.

The attachment efficiency (α) was employed to calculate critical coagulation concentrations (CCC) to make a quantitative description of aggregation kinetics of PS-NPs. α was calculated by normalizing the aggregation rate constant k (acquired in a certain suspension) to the rate constant at the fast aggregation conditions k_{fast} (obtained in the diffusion limited aggregation regime, where the aggregation rate was independent on electrolyte concentrations) (Eq. 2):

$$\alpha = \frac{k}{k_{fast}} = \frac{\left(\frac{dD_h(t)}{dt}\right)_{t\to 0}}{\left(\frac{dD_h(t)}{dt}\right)_{t\to 0,\ fast}} \tag{2}$$

Eventually, the experimental CCC values were determined from the intersect of extrapolated lines through the diffusion and reaction limited regimes.

The Derjaguin-Landau-Verwey-Overbeek (DLVO) theory with particle-particle model was used to give further elucidation of the observed results. Under various chemical conditions, the interaction energy, including van der Waals attraction $V_A(h)$, and electrostatic double-layer (EDL) repulsion $V_R(h)$, were calculated [21–23]. The total interaction energy $V_T(h)$ was calculated using the following equations (Eqs. 3–8):

$$V_T(h) = V_A(h) + V_R(h) \tag{3}$$

$$V_A = -\frac{A_{PWP}R}{12h}\left[1 - \frac{bh}{\lambda}\ln\left(1 + \frac{\lambda}{bh}\right)\right] \tag{4}$$

$$V_R^{\psi}(h) = \frac{2\pi R n_\infty k_B T \phi^2}{\kappa^2}\left[\ln\left(\frac{1+e^{-\kappa h}}{1-e^{-\kappa h}}\right) + \ln\left(1-e^{-2\kappa h}\right)\right] \tag{5}$$

$$n_\infty = 1000 N_A C_S \tag{6}$$

$$\phi = ze\varphi/k_B T \tag{7}$$

$$\kappa = \sqrt{\frac{e^2 \sum_i n_i z^2}{\varepsilon k_B T}} \tag{8}$$

where A_{PWP} was the combined Hamaker constant for PS-NPs interacting through water for a PS-water-PS system, and the Hamaker constants of PS-L-NPs and PS-S-NPs were 3.5×10^{-21} J and 2.3×10^{-21} J respectively [23]. $b = 5.32\lambda$ was the characteristic wavelength of the interaction with an often assumed value of 100 nm. R was the radius of PS-NPs. h was separation distance between particles, which was much smaller than their radius ($h << R$). k_B was the Boltzmann constant with a value of 1.381×10^{-23} J/L, and T was the absolute temperature. n_∞ was the bulk number density of ions. N_A was Avogadro constant with a value of 6.022×10^{-23}. C_S was the electrolyte molar concentration (mol/L). ϕ was the reduced potential. z was the valence of ion in the bulk suspension. e was the electron charge (1.60×10^{-19} C). φ was the electrical potential of PS-NPs, and was usually expressed as the ζ potential. κ was the Debye-Huckel reciprocal length at approximately 25 °C in aqueous solution. ε_0 was the permittivity of a vacuum (8.854×10^{-12} C V^{-1} m^{-1}). ε was the dielectric constant or relative permittivity of the solvent (78.5 for water). n was the number concentration of electrolyte.

Fig. S1 (Supporting information) presents the FT-IR spectra of PS-L-NPs and PS-S-NPs. Peaks at 700, 750, and 3020 cm^{-1} were designated to the benzene ring structure, and those peaks at 1490 and 1450 cm^{-1} were ascribed to the aromatic C–H deformation [24,25]. The broad and sharp bands at 1600 and 2920 cm^{-1} were attributed to the stretching vibration of aromatic C=C group and deformation of aliphatic C–H group, respectively [26]. Peak at 3450 cm^{-1} was ascribed to hydroxyl stretching, originated from water adsorption [27]. The peak at 1700 cm^{-1} for PS-S-NPs probably contributed to C=O group related to the presence of carboxyl groups [28].

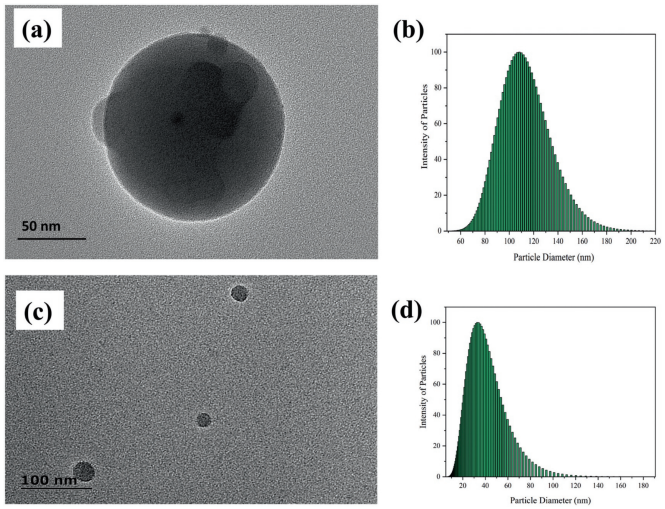

Fig. 1. TEM images and hydrodynamic size distributions of PS-L-NPs (a, b), and PS-S-NPs (c, d).

The size and shape of PS-L-NPs were detected by TEM, and it showed that PS-L-NPs had a spherical shape with an average diameter of 100 nm (Fig. 1a). The hydrodynamic size distribution of PS-L-NPs measured by DLS was ranged from 80 nm to 150 nm with an average diameter of 110 nm (Fig. 1b). The morphology of PS-S-NPs was also confirmed by TEM (Fig. 1c). The hydrodynamic size distribution of PS-S-NPs was ranged from 20 nm to 70 nm with an average diameter of 33 nm (Fig. 1d).

To assess the effect of pH on PS-NPs aggregation, the attachment efficiencies (α) of PS-L-NPs and PS-S-NPs with different concentrations of NaCl were calculated and displayed in Fig. 2. When α approaches to 1, the aggregation process is regarded as diffusion-limited [29]. Different solution pH (3, 6 and 8) led to differences in the aggregation profiles, and a higher pH value hindered the approaching of α to 1. Correspondingly, the experimental CCC of NaCl for PS-L-NPs at pH of 3, 6 and 8 were 193.86 mmol/L, 349.06 mmol/L and 470.41 mmol/L, respectively, and for PS-S-NPs were 380.13 mmol/L, 540.44 mmol/L and 755.26 mmol/L, respectively. There was a strong linear correlation between CCC and pH value (Fig. S2 in Supporting information). From this data, the aggregation of PS-NPs was suppressed with decreasing the solution pH, which is consistent with the phenomenon reported in previous study [30]. The DLVO theoretical calculations were accorded with the experimental CCC values under different pH conditions. As shown in Fig. S3 (Supporting information), the energy barrier decreased with increasing the concentration of NaCl, which is also reported by other studies [31].

Previous studies have indicated the protonation and deprotonation on the surface of PS-NPs play an important role in the aggregation behavior [32]. Therefore, the zeta potential of PS-NPs was measured and it was found that the zeta potential became more negative with increasing the pH values (Fig. S4 in Supporting information). For example, the zeta potential of PS-L-NPs in NaCl solution of 400 mmol/L decreased from −6.69 mV to −14.97 mV with increasing the pH from 6 to 8 (Fig. S4a), indicating that electrostatic repulsion between PS-NPs could be increased under alkaline conditions, which may reduce the aggregation between nanoplastics particles. It is suggested that the surface of PS-NPs could be easily deprotonated with increasing the pH, leading to improved stability of PS-NPs [33].

For convenience, the subsequent aggregation experiments were carried out at pH 6. Fig. 3 presents the increases of hydrodynamic diameter of PS-NPs along time with different types and concentrations of cations. In the presence of low concentration of cations, like 100 mmol/L NaCl, PS-NPs kept a relative stability due to the dominance of electrostatic repulsive forces [14]. With the increase of cation concentration, hydrodynamic diameter of PS-NPs increased quickly. According to the DLVO theory, the addition of cations led to characteristic adsorption and charge neutralization, where van der Waals forces dominated and the repulsion barrier was compressed. Thus, it was shown in Fig. S3 that the energy barriers of PS-NPs had been weakened as the cation concentration increased. When the cation concentration reached the CCC value, the PS-NPs were extremely unstable due to diffusion limitation, which eventually led to agglomeration between particles (Fig. S5 in Supporting information).

Compared the effects of mono- and divalent cations on PS-NPs aggregation, it is found that divalent cations were easier to induce the aggregation of PS-NPs relative to monovalent cations. For instance, the CCC values of NaCl and KCl for PS-L-NPs were ranged from 232.60 mmol/L to 349.06 mmol/L, while those of $MgCl_2$, $CaCl_2$ and $Pb(NO_3)_2$ were reduced to 16.25–40.31 mmol/L (Fig. S5). The ratio between the CCC values of Ca^{2+} and Na^+ was proportional to $z^{-3.37}$ (where $z = 2$ was the counterion valence for calcium) (Table S1 in Supporting information), consisting with the Schulze-Hardy Rule [34]. For the differences in CCC values of cations with the same valence state, a possible explanation was ascribed to the hydration layer forming between metal cations and water molecules. In other words, cations with larger radii tend to interact with more water molecules [30,35], thus producing a higher promotion effect on the aggregation of PS-NPs. Correspondingly, the promotion effects of divalent cations were in the same order with their radii: $Pb^{2+} > Ca^{2+} > Mg^{2+}$ (Table S1).

At present, a large number of studies have reported the size effect on the agglomeration and stability of nanoparticles, however, the size effect on the aggregation of PS-NPs has not been investigated explicitly in the existing literature [36–40]. The DLVO theory predicts a marked decrease in rates of coagulation of colloidal particles with an increase in particle size [41]. In this study, the CCC values of divalent ions (Ca^{2+}, Mg^{2+} and Pb^{2+}) for PS-S-NPs were lower than for PS-L-NPs (Fig. S5), which agreed with DLVO prediction. This revealed that the PS-L-NPs needed a higher concentration of divalent cations to break the stable state. The more negative zeta potential of PS-L-NPs relative to PS-S-NPs also confirmed the recalcitrance of PS-L-NPs to aggregation (Fig. S4). Besides, a common view was that higher adsorption rate of divalent cations occurred on the smaller particle, owing to the higher Gibbs free energy associated with the smaller particles. Figs. 4 and 5 present the TEM and EDX spectra of PS-NPs after the aggregation experiments with Pb^{2+}. From Fig. 4a, we can see that PS-L-NPs strikingly aggregated each other. At the same time, the EDX spectra showed the enrichment of Pb on the surface of PS-L-NPs, indicating that Pb^{2+} cations were adsorbed on PS-L-NPs (Figs. 4b-d). This characterization demonstrated the important role of Pb^{2+} in the induction of PS-NPs aggregation by the charge neutralization. Relatively, after the aggregation experiment with Pb^{2+}, the PS-S-NPs agglomerated closely into larger particles (>1 μm) and the surfaces were studded with Pb (Fig. 5). This result demonstrated a stronger adsorption capacity of PS-S-NPs for Pb^{2+}, which might be the key reason to explain the higher aggregation potential of smaller PS-NPs relative to larger PS-NPs with divalent cations.

However, for the monovalent cation system, the larger PS-NPs showed a higher tendency to aggregate, which is different with the situation in divalent cation system. The CCC values of Na^+ and K^+ for PS-L-NPs were 349.06 mmol/L and 232.60 mmol/L, which were smaller than that for PS-S-NPs (540.44 mmol/L and 412.66 mmol/L) (Fig. S5). By comparison on the zeta potential of PS-NPs (Fig. S4), PS-S-NPs had more negative charges in the same concentration of NaCl solution, indicating the smaller size of PS-NPs were in-

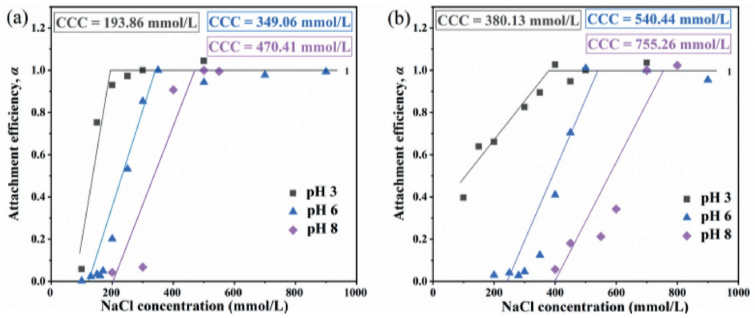

Fig. 2. Attachment efficiencies (α) of PS-L-NPs (a) and PS-S-NPs (b) with different concentrations of NaCl at different solution pH.

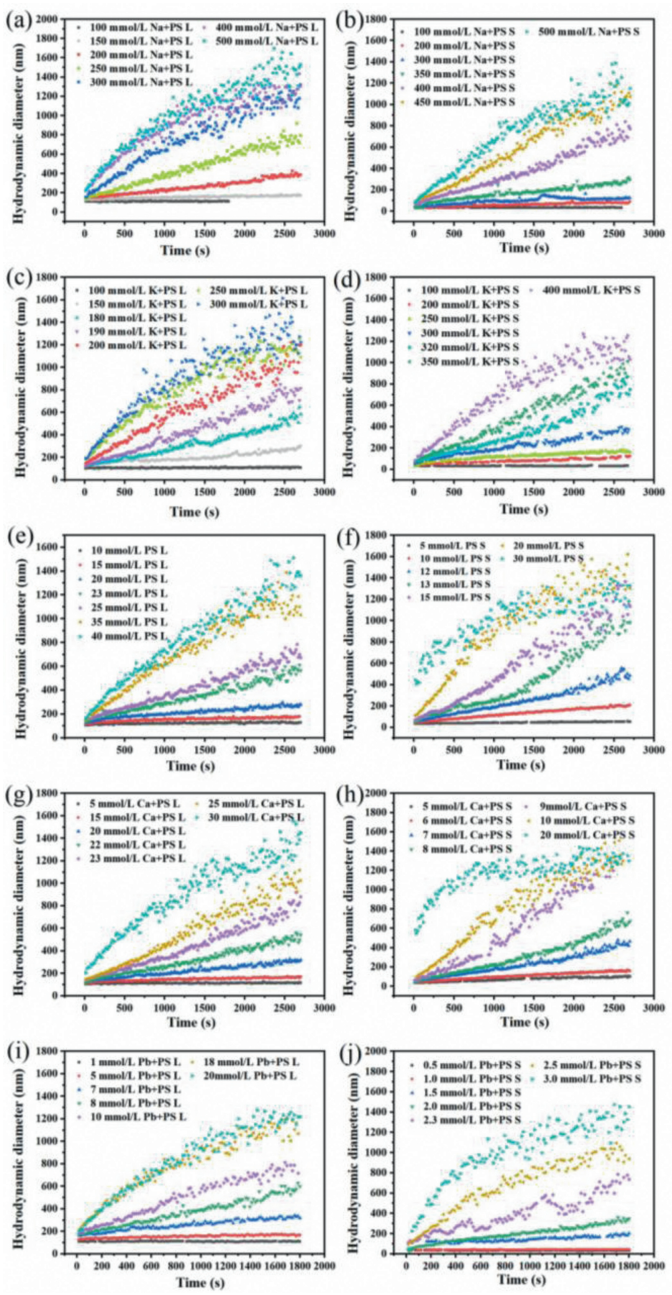

Fig. 3. Aggregation kinetics of PS-L-NPs (left) and PS-S-NPs (right) with different concentrations of NaCl (a, b), KCl (c, d), $CaCl_2$ (e, f), $MgCl_2$ (g, h) and $Pb(NO_3)_2$ (i, j) at pH 6.

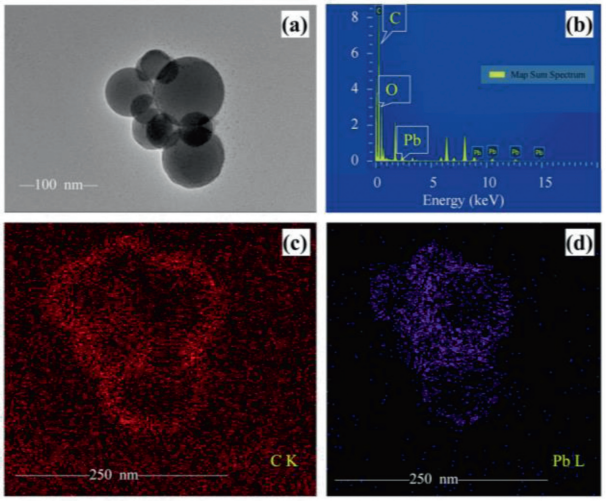

Fig. 4. The characterization of PS-L-NPs aggregates with $Pb(NO_3)_2$: (a) TEM image, (b) EDX spectrum, and mapping for element of carbon (c) and lead (d).

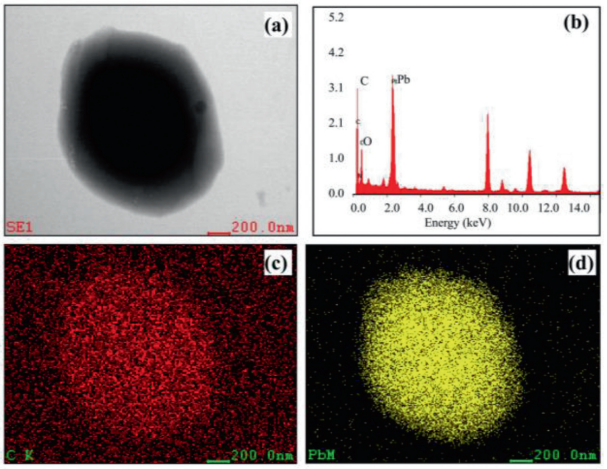

Fig. 5. The characterization of PS-S-NPs aggregates with $Pb(NO_3)_2$: (a) TEM image, (b) EDX spectrum, and mapping for element of carbon (c) and lead (d).

deed more stable. In fact, there are differences between studies exploring size effect on the stability of nanoparticles, even finding that the stability of colloid is insensitive to particle size [40]. For instance, Afshinnia, Sikder, Cai and Baalousha [39] observed a negatively strong association between the CCC and particle size of nano-silver for monovalent cations, but no clear trend was observed for divalent cations. Deposition in secondary minimum and the narrow range of surface potential were used to ex-

plain the observed anomalous particle size effect. In DLVO theory, the surface charge of particles is assumed to be distribution uniformly, that all particles have a constant surface potential [41]. In other words, it is most likely that the discrepancies with respect to particle size effects are related to the failure of the DLVO theory to consider hydrodynamic interaction and dynamics of interaction.

In conclusion, this study set out to systematically explore the aggregation kinetics of different sizes of PS-NPs with monovalent (Na^+, K^+) and divalent (Ca^{2+}, Mg^{2+} and Pb^{2+}) cations at different solution pH. The primary results of this investigation are summarized as follows: (1) Due to deprotonation, PS-NPs were more stable in alkaline conditions. (2) Compared with monovalent cations, divalent cations have a greater effect on the stability of PS-NPs; the hydration ability of cations with the same valence state led to the difference in the stability of PS-NPs. (3) The smaller size of PS-NPs in monovalent cation system was more stable but easier to agglomerate in divalent cation system, and there were other unknown factors that DLVO theory does not consider affect the stability of NPs with different particle sizes.

Declaration of competing interest

The authors declare that they have no known competing financial interests or personal relationships that could have appeared to influence the work reported in this paper.

Acknowledgments

The project is supported by Scientific Research Project of Guangzhou University (No. YK2020017), the Program Foundation of Institute for Scientific Research of Karst Area of NSFC-GZGOV (No. U1612442), Research Grants Council of the Hong Kong Special Administrative Region, China (No. UGC/IDS(R)16/19), Industry-University Cooperation and Collaborative Education Project of the Ministry of Education of the People's Republic of China (No. 202101134012) and Innovative training program for College Students of Guangzhou University (No. S202111078039).

Supplementary materials

Supplementary material associated with this article can be found, in the online version, at doi:10.1016/j.cclet.2022.01.056.

References

[1] J.P.G.L. Frias, R. Nash, Mar. Pollut. Bull. 138 (2019) 145–147.
[2] Plastics Europe, Plastics-the Facts: an analysis of European plastic production, demand and waste data, Brussels, 2019.
[3] K. Mattsson, L.A. Hansson, T. Cedervall, Environ. Sci.: Processes Impacts 17 (2015) 1712–1721.
[4] M. Niaounakis, Management of Marine Plastic Debris, William Andrew Publishing, Holland, 2017.
[5] S. Lambert, C. Sinclair, A. Boxall, Rev. Environ. Contam. Tocicol. 227 (2014) 1–53.
[6] C.J. Moore, Environ. Res. 108 (2008) 131–139.
[7] I. Brandts, M. Teles, A.P. Gonçalves, et al., Sci. Total Environ. 643 (2018) 775–784.
[8] Q. Chen, D. Yin, Y. Jia, et al., Sci. Total Environ. 609 (2017) 1312–1321.
[9] C. González-Fernández, K. Tallec, N.Le Goïc, et al., Chemosphere 208 (2018) 764–772.
[10] X. Li, E. He, K. Jiang, et al., Water Res. 190 (2021) 116742.
[11] Y. Liu, Z. Huang, J. Zhou, et al., Water Res. 186 (2020) 116316.
[12] O. Oriekhova, S. Stoll, Environ. Sci. Nano 5 (2018) 792–799.
[13] S. Yu, M. Shen, S. Li, et al., Environ. Pollut. 255 (2019) 113302.
[14] L. Cai, L. Hu, H. Shi, et al., Chemosphere 197 (2018) 142–151.
[15] M. Davranche, C. Veclin, A.C. Pierson-Wickmann, et al., Environ. Pollut. 249 (2019) 940–948.
[16] C.M. Rochman, B.T. Hentschel, S.J. Teh, et al., PLoS One 9 (2014) e85433.
[17] D.J. Sarkar, S. Das Sarkar, B.K. Das, et al., Water Res. 192 (2021) 116853.
[18] A. Karami, Chemosphere. 184 (2017) 841–848.
[19] Q. Wu, H. Li, X. Hu, et al., Chin. Chem. Lett. 31 (2020) 2825–2830.
[20] K.L. Chen, M. Elimelech, J. Colloid Interface Sci. 309 (2007) 126–134.
[21] J. Gregory, J. Colloid Interface Sci. 83 (1981) 138–145.
[22] R. Hogg, T.W. Healy, D.W. Fuerstenau, et al., Trans. Faraday Soc. 62 (1966) 1638–1651.
[23] Y. Liu, Y. Hu, C. Yang, et al., Water Res. 163 (2019) 114870.
[24] B.C. Kim, S. Nair, J. Kim, et al., Nanotechnology 16 (2005) S382–S388.
[25] S. Zhu, D. Yan, G. Zhang, Polym. Bull. 45 (2001) 457–464.
[26] B. Hu, Q. Hu, D. Xu, et al., Sep. Purif. Technol. 175 (2017) 140–146.
[27] H. Sertchook, D. Avnir, Chem. Mat. 15 (2003) 1690–1694.
[28] P. Govindaiah, Y.J. Jung, J.M. Lee, et al., J. Colloid Interface Sci. 343 (2010) 484–490.
[29] O.S. Alimi, J. Farner Budarz, L.M. Hernandez, et al., Environ. Sci. Technol. 52 (2018) 1704–1724.
[30] Y. Mao, H. Li, X. Huangfu, et al., Environ. Pollut. 258 (2020) 113760.
[31] A.R. Petosa, D.P. Jaisi, I.R. Quevedo, et al., Environ. Sci. Technol. 44 (2010) 6532–6549.
[32] S. Dong, W. Cai, J. Xia, et al., Environ. Pollut. 268 (2021) 115828.
[33] Q. Li, B. Chen, B. Xing, Environ. Sci. Technol. 51 (2017) 1364–1376.
[34] J. Masliyah, J. Colloid Interface Sci. 200 (1998) 195.
[35] J.I. Kilpatrick, S.-.H. Loh, S.P. Jarvis, J. Am. Chem. Soc. 135 (2013) 2628–2634.
[36] Z.F. Song, X.Y. Yang, F.M. Chen, et al., Sci. Total Environ. 669 (2019) 120–128.
[37] Y.T. He, J.M. Wan, T. Tokunaga, J. Nanopart. Res. 10 (2008) 321–332.
[38] M.J. Mulvihill, S.E. Habas, H. Jen-La Plante, et al., Chem. Mat. 22 (2010) 5251–5257.
[39] K. Afshinnia, M. Sikder, B. Cai, et al., J. Colloid Interface Sci. 487 (2017) 192–200.
[40] J. Liu, S. Legros, G. Ma, et al., Chemosphere 87 (2012) 918–924.
[41] M. Elimelech, C.R. O'Melia, Langmuir 6 (1990) 1153–1163.